DISCRETE ELEMENT MODELING OF STRENGTH PROPERTIES AND FAILURE MODES OF QH-E LUNAR SOIL SIMULANT AT LOW CONFINING STRESSES

Li Yun-Li [1], Zou Wei-Lie[1,2], Wu Wen-Ping[1] and Chen Lun[3]*

1. *Key Laboratory of Geotechnical and Structural Engineering Safety of Hubei Province, School of Civil Engineering, Wuhan University, Wuhan 430072, China; liyunli @whu.edu.cn*

2. *School of Civil Engineering, Xijing University, Xi'an 710123, China; zwilliam @126.com*

3. *State Key Laboratory of Hydroscience and Engineering, Tsinghua University, Beijing 100084, China; lunchen @mail.tsinghua.edu.cn*

ABSTRACT

In this paper, discrete element method (DEM) is used to investigate the strength properties and failure modes of QH-E lunar soil simulant at the low confining stress. The deviator stress-axial strain curves and volumetric strain-axial strain curves are obtained based on DEM simulations, which are basically consistent with the experimental results at the low confining stresses, and the lower confining stress is, the closer to the experimental curves will obtain. Moreover, for a given low confining stress, the effects of porosity and friction coefficient on strength properties of QH-E samples are discussed. The results show that the peak stress, residual stress and axial strain corresponding to the peak stress obviously decrease with the increase of the porosity, while slightly increase with the increase of the friction coefficient. Furthermore, the whole failure processes and failure modes at different low confining stresses are also observed by DEM simulations. The simulated results indicate that the V-type shear zone (double shear bands) is the main failure mode at the low confining stress, and then the V-type shear zone gradually changes to a single shear band (along the horizontal direction about 52°) with the increase of the confining stress.

KEYWORDS

Discrete element method, Triaxial compression test, Mechanical properties, Failure modes

INTRODUCTION

Manned lunar exploration has attracted renewed interest, many countries are preparing their own plans for lunar exploration [1]. The lunar soil will be the first lunar material that explorers and exploration equipment directly contact when they land on the Moon and its mechanical characteristics are important to lunar exploration. Because of the limited amount of lunar regolith brought back to Earth by the Apollo missions, lunar soil simulants, as the substitutions of real lunar soils, was developed to investigate the mechanical properties of real lunar soils [2-6], as well as the interaction behaviour between exploration equipment and lunar soils.

Particle flow code (PFC) numerical simulation as a discrete element method (DEM) is being constantly used in the research of the basic physical and mechanical properties of granular materials. The lunar soil consists of discrete solid particles, which can be classified as a granular material or similar to granular soil [2]. Many researchers investigated the mechanical properties of the lunar soil stimulants using PFC numerical simulation. For example, Hasan and Alshibli [1]

----

carried out PFC three-dimensional (PFC3D) modelling of the tri-axial compression test on lunar soil simulant JSC-1A, and discussed the effects of confining pressure, sample density and environment gravity on the shear strength of lunar soil simulant. Jiang *et al.* [7, 8] used PFC to simulate the biaxial compression test under flexible boundary conditions, and studied the influences of the ground environment (excluding van der Waals force) and lunar environment (including van der Waals force) on the formation process of shear zones. The results indicated that the peak strength and the residual strength of the samples with van der Waals force are relatively high in the compression process, and the lunar environment has a significant impact on the failure mode and characteristics (angle and thickness of shear bands) of the sample. Somrit and Nakagawa [9] simulated the formation process of the cement fusion in the high heat impact zone of the lunar surface when the micrometeorite hit the lunar surface by fitting the impact energy distribution equation into the PFC2D software. Tryana and Masami [10] established the numerical model of uniaxial compression test by considering the parallel cohesion between the particles to carry out the PFC modelling of cement in the lunar soil. The results showed that the cement content has a strong effect on the compression properties of lunar soil. Considering the irregular shape of actual lunar soil particles, Lee *et al.* [11] described DEM simulations with polyhedral particle shapes to reproduce experimental tests on JSC-1A lunar soil simulant. Katagiri *et al.* [12] developed three-dimensional (3D) grain shape characteristics of returned lunar soil and its numerical simulation by using the image-based DEM. The grain shapes were modelled by clumping 10 spheres in the image-based DEM simulations. Matsushima *et al.* [13, 14] proposed a dynamic optimization algorithm method to simulate the complex shape of the actual lunar soil particles, and carried out PFC modelling of study the influence of the micro-parameters such as the indirect contact stiffness, elastic constant and friction coefficient on the forming process of the angle of repose. Furthermore, the interaction behaviour between exploration equipment and lunar soils was also investigated by DEM numerical simulations [16-19]. Smith and Peng [17] found that surface roughness significantly influence vehicle mobility and efficiency by DEM modelling of wheel-soil interaction over rough terrain. Zou *et al.* [18] carried out the plate-sinkage test and the track-shoe test to study the stress sinkage and shear properties of the lunar soil. The results indicated the load that the lunar soil can bear increases with the increase of the bearing area, but the bearing capacity weakens with the increase of the porosity. Li *et al.* [19] simulated the interaction between lunar regolith and wheel by considering the influence of the lunar low gravity environment. As in the DEM numerical simulation work mentioned above, it can be seen that the mechanical properties of lunar soil and the interaction between lunar soil and wheel (probe) are closely related to the lunar environment and micro-parameters of lunar soil.

The gravity on the Moon is about 1/6 of that on Earth, one of the problems demanding a solution is the mechanical properties of the lunar soil under the microgravity environment [20-23]. In other words, the lunar soil is subject to very low confining stresses under a microgravity environment conditions which the mechanical properties may differ from those observed under regular tests. In our previous work [24], the mechanical properties and deformation behaviour of QH-E lunar soil simulant at the low confining stresses and those of QH-E at the conventional confining stresses were systematically studied by laboratory test. The research results ascertained the mechanical properties of QH-E lunar soil simulant at lower confining stress and provided a reference and standard for the selection of micro-parameters of the DEM numerical simulation.

In this paper, the tri-axial compressive mechanical properties of QH-E lunar soil simulant at the low confining stress is further investigated by DEM simulation, and compares the simulation results with our previous experimental data [24]. The objective of the present work is to determine the mechanical properties and failure modes of QH-E at low confining stresses, and explore the effects of micro-parameters (porosity, friction coefficient) on mechanical properties. Especially, the failure processes and failure modes of QH-E under different low confining stress conditions are discussed based on DEM simulation.

SIMULATION MODEL

Selection of particle size and generation of numerical model

In our previous experimental tests, a type of lunar soil simulant named as QH-E was developed by Tsinghua University to investigate the properties of the lunar soil [24]. In the present DEM simulations, the same physical parameters of QH-E lunar soil simulant are selected to further investigate the mechanical properties of QH-E by comparing with our previous experimental results. The grain-size analysis of QH-E was conducted according to ASTM D422-63 for particles greater than 0.075 mm in diameter, and the testing result is shown in Figure 1. As we all know in many DEM simulations, particles are commonly approximated by spherical or ellipsoidal shaped particles to keep the required computational resources manageable, and the spherical particle shape greatly simplifies simulations and accommodates the maximum number of particles for any given central processing unit (CPU) execution time budget [25]. In the present simulation, the shapes of particles are also considered to be spherical with the grain size of 1~1.5 mm for convenience of calculation and easily extract the fundamentals of deformation behaviour and failure modes of QH-E at the low confining stresses.
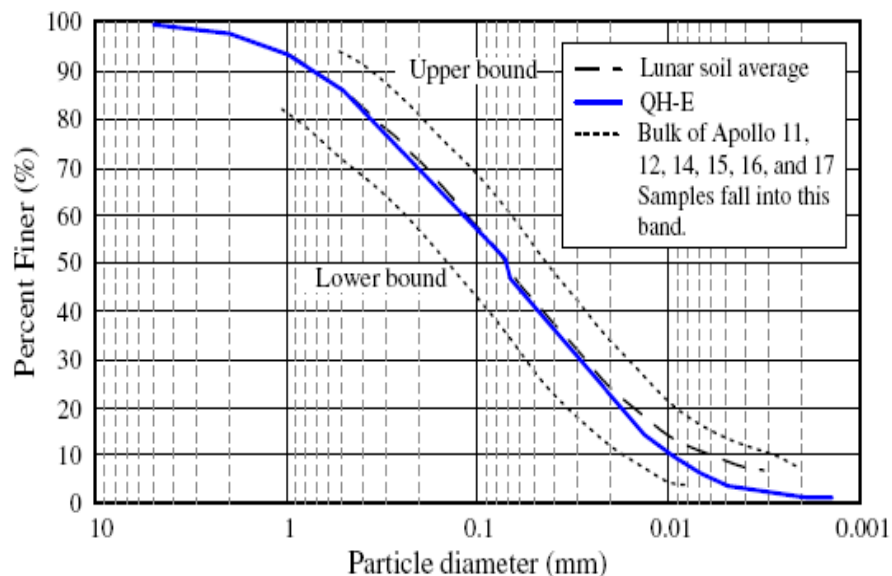

Fig. 1 - Particle size distribution curves of QH-E sample, the upper boundary, lower boundary, and average of bulk of Apollo samples [24].

Triaxial compression simulations are performed on the cylindrical soil samples using PFC3D numerical simulation following two steps: (1) inputting command stream in PFC3D to generate a 140 mm height and 70 mm diameter flexible cylinder and two rigid loading plates, which has the same size as the experimental sample. (2) Particle aggregation of simulation model in accordance with the aggregation of lunar soil simulant through PFC3D embedded fish language programming, as shown in Figure 2. In the present simulations, the initial porosity of simulation model is 0.38, and the particle size is the range of 1~1.5 mm random distribution, 40980 particles are produced in the PFC3D model. So large number of particles maybe affect the calculating speed and computational time to a certain extent, but the stress-strain and volumetric strain curves outputted from PFC3D are more uniform.
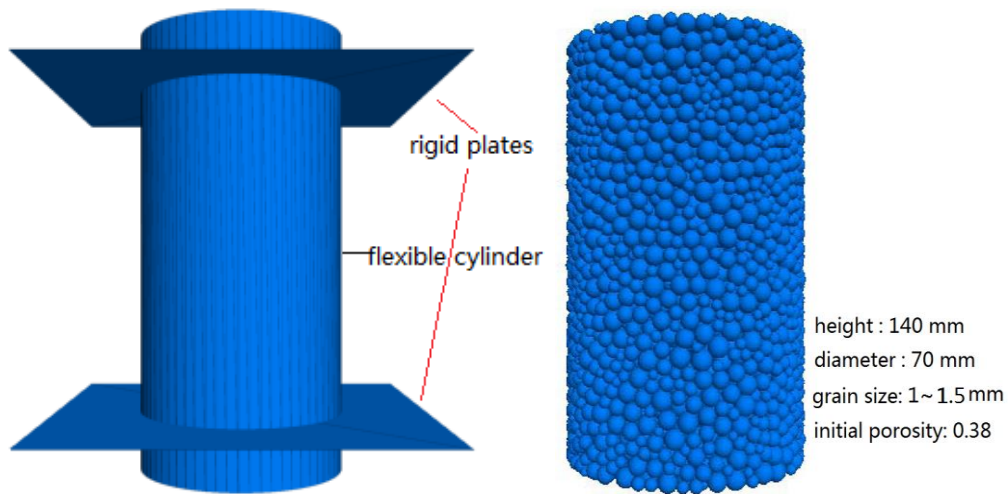

Fig. 2 - Model geometry for PFC3D simulation

Contact constitutive model

In the geotechnical problem of lunar soil PFC numerical simulation, the contact constitutive model is generally adopted to calculate the interaction force between particles in the PFC software. The normal and tangential contact stiffness of the particles can be determined according to their own stiffness and contact mechanics model. Due to the fact that lunar soil has a certain amount of apparent cohesion [26, 27], parallel-bonded model is used to study the tri-axial compression mechanical properties of lunar soil simulant, which has been successfully applied to simulate mechanical properties of lunar soil simulant [28, 29].
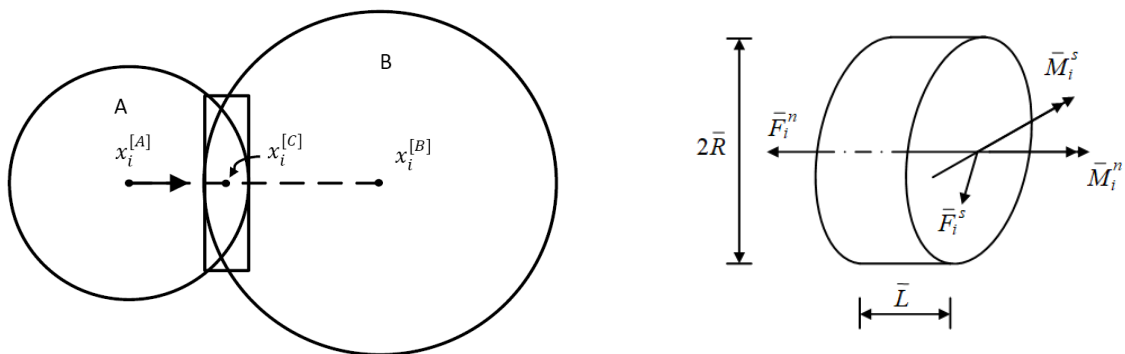

Fig. 3 - Schematic diagram of parallel bond model and its force and torque distribution

Figure 3 shows schematic diagram of parallel bond model and its force and torque distribution. The contact part between the two elements is considered to be a disc, which is expressed in a spring with normal and tangential stiffness. This group of springs are uniformly distributed in the contact plane. Due to the existence of the parallel bond stiffness, after this kind of bond is produced, the contact at the relative motion in the adhesive materials induces a force and a torque, the forces and moments acting on the two bonded particles and related to the maximum normal and tangential stress of the material bonded edges. If either of the maximum stress exceeds the corresponding bond strength, the parallel bond is broken. Parallel bond is defined by five parameters: normal stiffness $\bar{k}_n$, tangential stiffness $\bar{k}_s$, normal strength $\bar{\sigma}_n$, tangential strength $\bar{\sigma}_s$ and adhesive disc radius $\bar{R}$, respectively. The normal and tangential stresses of parallel-bonded model are expressed as follows:

The increment of normal and tangential components of the contact force:

$$\overline{F}_n := \overline{F}_n - \overline{k}_n \overline{A} \cdot \Delta U_n$$

$$\overline{F}_s := \overline{F}_s - \overline{k}_s \overline{A} \cdot \Delta U_s$$

(1)

where $\overline{A}$ is the contact area; ΔU_n, ΔU_s is the normal and tangential increment for the contact displacement within the time step, respectively. The increment of the contact displacement ΔU_i is given by:

$$\Delta U_i = V_i \Delta t$$

(2)

The contact moment is divided into two parts, the torque and the moment:

$$\overline{M}_i = \overline{M}_i^n \cdot \hat{n} + \overline{M}_i^s$$

(3)

The torque and moment are described as:

$$\overline{M}_i^n := \begin{cases} 0.0 & , 2D \\ \overline{M}_i^n - \overline{k}_s \overline{J} \Delta \theta_i^n & , 3D \end{cases}$$

(4)

$$\overline{M}_i^s := \overline{M}_i^s - \overline{k}_n \overline{I} \Delta \theta_i^s$$

where $\overline{J}$ is the moment of inertia of the disc cross section, $\overline{I}$ is the moment of inertia of the contact surface along the $\Delta \theta_i^s$ direction axis and via contact point. $\Delta \theta_i$ is determined by

$$\Delta \theta_i = (\omega_i^{[B]} - \omega_i^{[A]}) \Delta t$$

(5)

Based on Moore-Kulun failure criterion, the $\overline{\sigma}$, $\overline{\tau}$, $\overline{\tau}_c$ are expressed as

$$\overline{\sigma} = \frac{\overline{F}_n}{\overline{A}} + \overline{\beta} \frac{\left\| \overline{M}_i^s \right\| \overline{R}}{\overline{I}}$$

(6)

$$\overline{\tau} = \frac{\left\| \overline{F}_s \right\|}{\overline{A}} + \begin{cases} 0 & , 2D \\ \overline{\beta} \frac{\left| \overline{M}_i^n \right| \overline{R}}{\overline{J}} & , 3D \end{cases}$$

$$\overline{\tau}_c = \overline{c} - \overline{\sigma} \tan \overline{\varphi}$$

Micro-parameters calibration for PFC simulation

Model parameters required in a PFC numerical simulation can be classified into two categories: 1) physical parameters characterizing the geometrical size of the sample and the experimental conditions; 2) microscopic parameters characterizing particles and their contact mechanics model. The values of the physical parameters can be directly determined by the actual situation of the experiment, while microscopic parameters need to be calibrated which would be a very tedious and time consuming process. The simulation of the tri-axial test (in 3D) or the biaxial test (in 2D) is the basic method to determine the microscopic parameters of the PFC model. Through repeatedly adjusting the input of the microscopic parameters of the model, the simulation results are in agreement with the experiment results as much as possible, so as to determine the values of the parameters, and to further carry out other numerical simulation research. The

----

physical and microscopic parameters of the QH-E lunar soil simulant were calibrated as shown in Table 1.

Tab. 1 - Parameters for PFC tri-axial compression numerical simulation

Parameters	Values	Parameters	Values
Porosity e	0.38	Normal stiffness $\bar{k}_n$ （N/m）	1.0e8
Particle size $2\bar{R}$ （mm）	1~1.5	Tangential stiffness $\bar{k}_s$ （N/m）	0.85e8
Friction coefficient f	0.25	Normal strength $\bar{\sigma}_n$ （N/m）	1.0e5
Particle density ρ （kg/m³）	1640	Tangential strength $\bar{\sigma}_s$ （N/m）	1.0e5

The two other parameters of cohesion and internal friction angle need to be determined by the stress strength values of the experimental results. According to the experimental data draw the Mohr's circle and their common tangent, and then obtain cohesion and internal friction angle. The cohesion is 3.1kPa ($\bar{c}$ =3.1kPa) and internal friction angle is 51.55^0 ($\bar{\varphi}$=51.55^0).
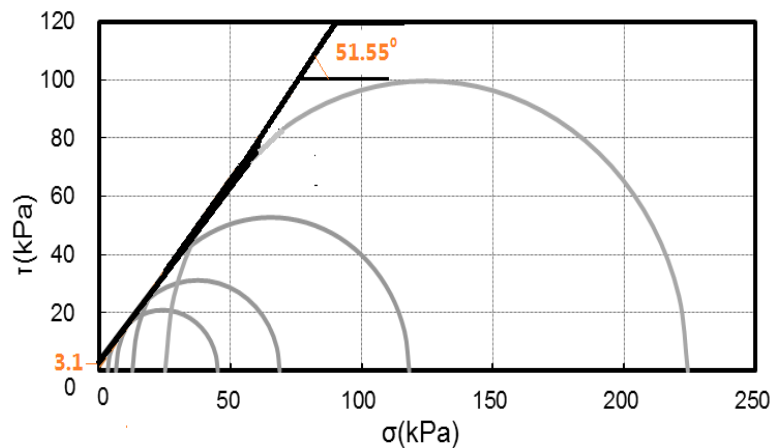

Fig. 4 - The strength envelope of QH-E lunar soil simulant

SIMULATION RESULTS AND DISCUSSION

Deviator Stress- Axial Strain curves

Figures 5(a)-(c) show the deviatoric stress versus axial strain relationship for QH-E samples at the low confining stresses of 6.25, 12.5, and 25 kPa, respectively. The stress-strain curves can be divided into three stages: hardening stage before the peak deviatoric stress, rapid softening stage after peak deviatoric stress, and the residual stress stage after softening. The peak deviatoric stress increases with the increase of the confining stress, and the amount of postpeak softening also increases with the increase of the confining stress (see Figure 5). It is also shown that QH-E lunar soil simulant displayed a significant strain-softening behaviour associated with the development of a shear band as shown in Section 4. The strain softening contributed to an approximatively equal residual strength, and the residual strength envelopes of QH-E are approximately linear. With the increase of confining stress, the axial strain corresponding to peak stress becomes larger. Comparison of the simulation curves and experimental curves, the deviator stress versus axial strain curves are basically consistent in the elastic deformation stage, the

----

magnitudes of stress in the plastic softening stage have slightly smaller than those of experimental results, but have the same deformation trend as shown in Figure 5.

Table 2 shows the values of peak deviatoric stress, residual stress and axial strain corresponding to the peak stress at low confining stresses based on both PFC3D simulation and experimental results. As can be seen in Table 2, the simulated peak deviatoric stress, residual stress and axial strain at peak stress are close to those of experimental results. Moreover, from Figure 5 and Table 2, we found the deviatoric stress-axial strain curves and values of peak stress, residual stress and axial strain are closer to the experimental results at the lower confining stress. It indicated that the proposed parallel-bonded model and calibrated microscopic parameters are able to represent the mechanical behaviour of QH-E lunar soil simulant at the low confining stresses. It is also emphasized that the values of peak deviatoric stress, residual stress and axial strain at peak stress are slightly smaller than those of experimental values, and the deviation gradually becomes larger with the increase of confining stress, which could be related to the model without considering the particle shape features. It is shown that QH-E lunar soil simulant is of angular shape with sharp corners and a highly irregular surface because of the Raymond mill method used to grind QH-E [24]. In the tri-axial compression tests, the irregular particle shape can increase the shear strength [11, 30]. Therefore, the simulated values of peak deviatoric stress, residual stress and axial strain at peak stress are slightly smaller than those of experimental results.
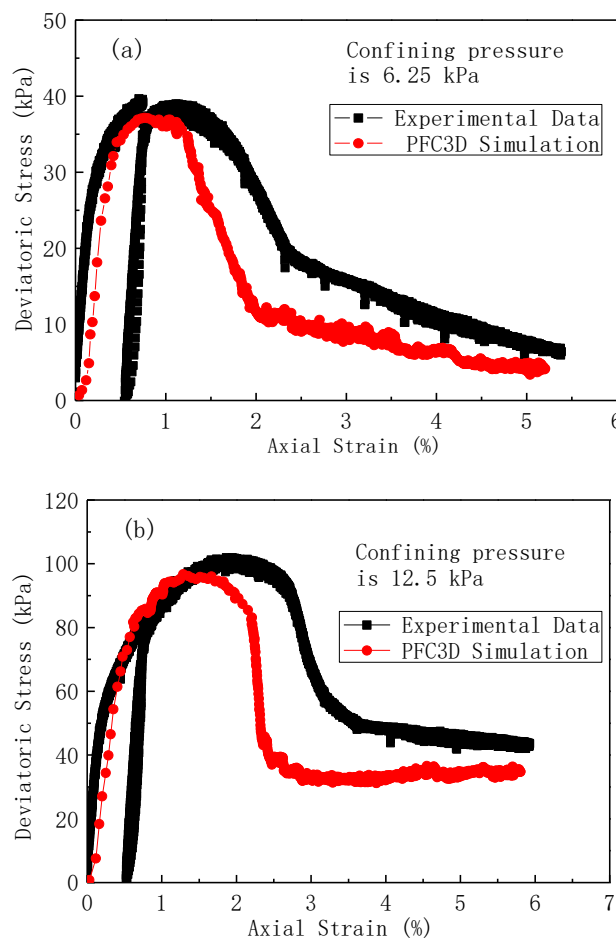

Fig. 5 - The deviatoric stress versus axial strain curves and comparison with experimental curves at the low confining stresses of (a) 6.25 kPa, (b) 12.5 kPa,
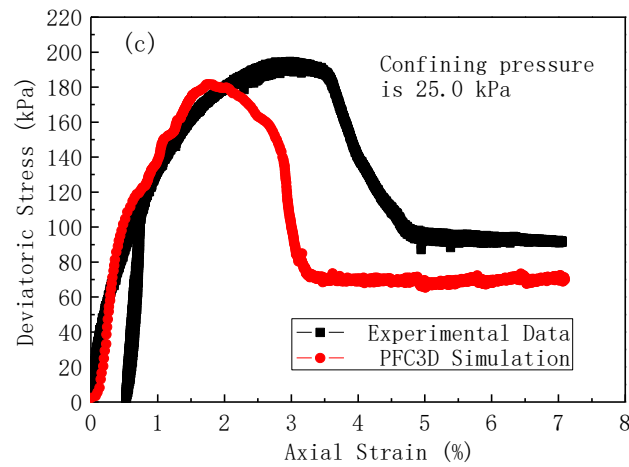
Fig. 5 - The deviatoric stress versus axial strain curves and comparison with experimental curves at the low confining stresses of (c) 25 kPa, respectively

Tab. 2 - Comparison of the simulation results and experimental results

Confining stress (kPa)	Peak deviatoric stress (kPa)		Axial strain at peak stress (%)		Residual stress (kPa)	
	Simulation results	Experimental results	Simulation results	Experimental results	Simulation results	Experimental results
6.25	37.2	40.1	0.75	0.78	6.5	7.5
12.5	98.3	101.6	1.46	1.58	38	43
25.0	181.5	188.2	1.83	2.42	75	88

Volumetric Strain- Axial Strain curves

Figures 6(a)-(c) show the simulated volumetric strain versus axial strain and comparison with experimental curves at low confining stresses of 6.25, 12.5, and 25kPa, respectively. It can be observed that the larger the confining stress, the smaller the ultimate value of the volumetric strain because of the stronger confining restraint. At low confining stresses of 6.25, 12.5, and 25kPa, the samples displayed highly dilative behaviour since the beginning of loading. The lower the confining stress is, the stronger the dilatancy is, and the greater the volumetric strain is. Further, it can be found that the volumetric strains of the samples at low confining stresses do not tend toward stability, and the samples do not exhibit constant critical state volumes (see Figure 6). The volumetric strains will gradually tend toward stability with the increase of the confining stress. By comparison with experimental curves, it can be seen that the PFC3D simulations of volumetric strain versus axial strain curves show an overall good agreement with experimental curves, and the lower the confining stress is, the simulated curves are closer to the experimental curves. It further reveals that the proposed parallel-bonded model and calibrated microscopic parameters are feasible for studying the mechanical properties of QH-E lunar soil simulant at the low confining stresses.

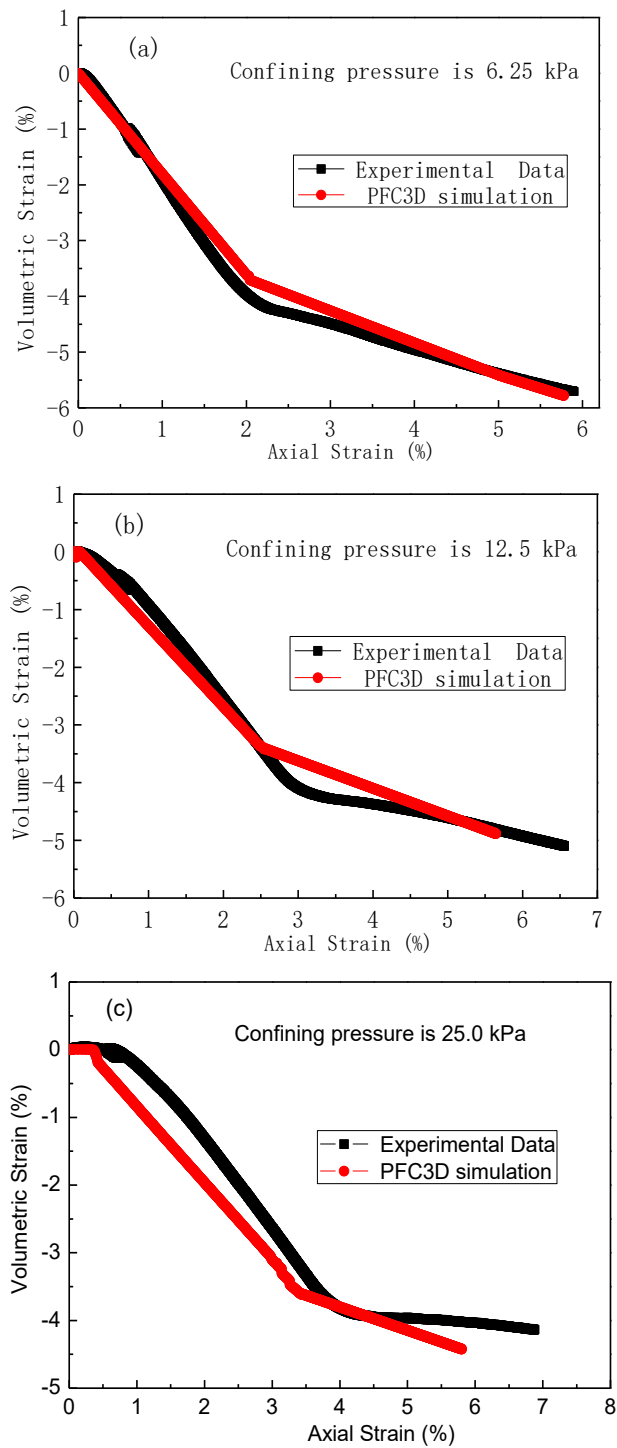

Fig. 6 - The volumetric strain versus axial strain curves and comparison with experimental curves at the low confining stresses of (a) 6.25kPa, (b) 12.5kPa, and (c)25kPa, respectively.

Effects of porosity and friction coefficient on stress-strain curves

Figure 7 shows the deviatoric stress and axial strain relationship at different porosities and friction coefficients for the same confining stress of 25.0kPa, respectively. As seen in Figure 7, the peak deviatoric stress and residual stress increased in the stress-strain curves with increasing the friction coefficient, whereas decreased with increasing the porosity, and the initial elastic modulus also increased slightly with increasing the friction coefficient or decreasing the porosity. Zou *et al.* (2008) studied the effect of micro-parameters on the statics characteristic of lunar soil at the conventional confining stress through PFC3D simulation of tri-axial compression test. Their simulation results show that with increasing the friction coefficient, the peak stress increases obviously, and it increases slightly with increasing the particle contact stiffness. While the peak stress decreases with increasing the porosity. The present results indicate that the effects of the porosity and the friction coefficient on the peak stress of QH-E lunar soil simulant at the low confining stress are the same as those at the conventional confining stress by Zou *et al.* [29].

Table 3 presents a quantitative relationship for the effects of friction coefficient and porosity on the peak stress, residual stress and axial strain corresponding to the peak stress. The peak stress, residual stress and axial strain corresponding to the peak stress are obviously increased with the decrease of the porosity, the peak deviator stress increased obviously from 87.5 to 466.2kPa, the residual stress increased from 36.5 to 156.5kPa, and the axial strain corresponding to this peak stress also increased from 1.35% to 2.25% when the porosity decreased from 0.42 to 0.3 at the same confining stress of 25.0kPa. The effect of friction coefficient is not as obvious as those of the porosity, the peak deviator stress increased from 172.4 to 205.0kPa and the residual stress increased from 67.5 to 77.6kPa when the friction coefficient increased from 0.20 to 0.40, while the change of the axial strain corresponding to the peak stress is very small (from 1.77% to 1.85%) as shown in Table 3.

It can be seen from Figure 7 that the porosity and friction coefficient can obviously affect the peak strength of QH-E lunar soil simulant, and porosity has a stronger effect on the peak strength for tri-axial compression simulation at low confining stress. It indicates that the requirements of macro-mechanical strength can be realized by adjusting the micro-parameters. In general, the initial porosity of the sample is given, so the requirement of the peak strength of tested sample can be achieved by changing the friction coefficient.
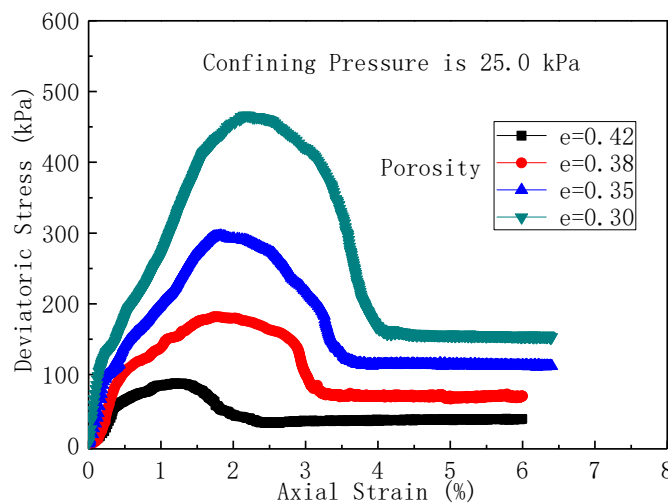

Fig. 7 - The deviatoric stress and axial strain relationships at different (a) porosities
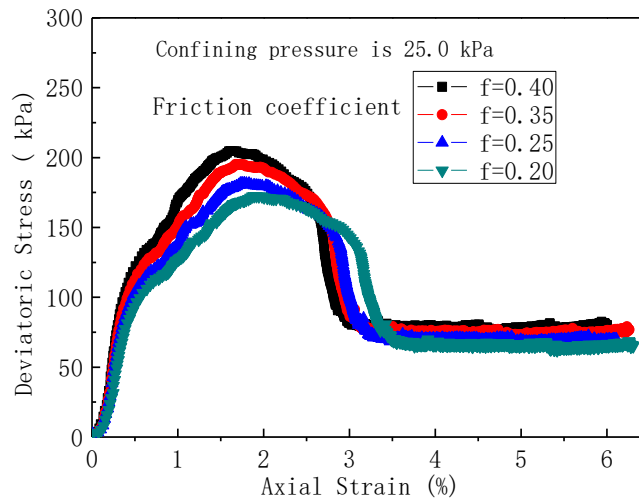

Fig. 7 - The deviatoric stress and axial strain relationships at different (b) friction coefficients

Tab. 3 - The peak deviatoric stress and corresponding axial strain at different porosities and friction coefficients

Macroscopic mechanical response	Porosity				Friction coefficient			
	e=0.30	e=0.35	e=0.38	e=0.42	f=0.20	f=0.25	f=0.35	f=0.40
Peak deviatoric stress (kPa)	466.2	296.4	181.5	87.5	172.4	181.5	195.3	205.0
Axial strain at peak stress (%)	2.25	1.98	1.83	1.35	1.85	1.83	1.79	1.77
Residual stress (kPa)	156.5	113.6	75.0	36.5	67.5	70.5	75.0	77.6

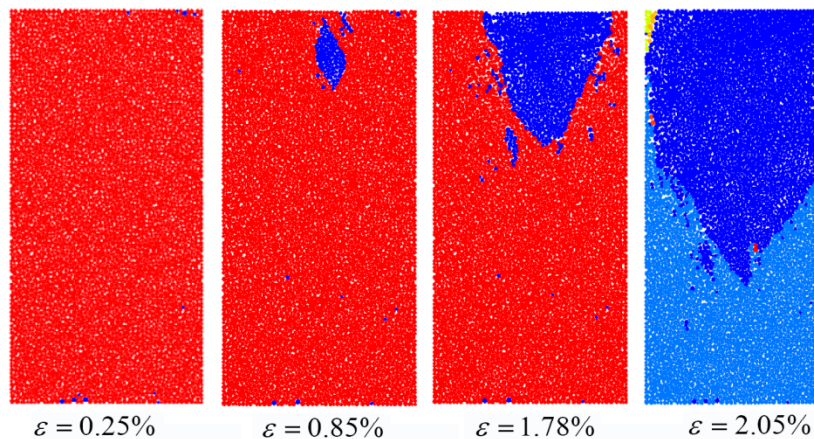## FAILURE PROCESSES AND FAILURE MODES AT LOW CONFINING STRESSES

Based on the discussion and analysis of the deviatoric stress versus axial strain and volumetric strain versus axial strain curves, it can be found that the proposed parallel-bonded model and calibrated microscopic parameters are feasible for studying the mechanical properties of QH-E lunar soil simulant at the low confining stresses. In order to more clearly observe the failure processes and failure mechanisms of specimen interior at different low confining stresses, a two-dimensional model is chosen to qualitatively simulate the failure mechanisms by using the above parallel-bonded model and microscopic parameters of QH-E lunar soil simulant at the low confining stresses, and the failure modes are recorded during the whole process of simulation.

Figure 8(a) shows the failure process and failure mode at the confining stress of 6.25kPa. A local damage occurs in the upper part of the sample at the axial strain of 0.2%, with the increase of the strain, the damage degree increases gradually, and the failure of QH-E lunar soil simulant is from the edge to the internal zone of the sample. Then, the V-type shear zone (double shear bands) appears in the upper part of the sample at the axial strain of 1.45%, and the V-type shear zone becomes larger with the increase of the strain (at the axial strain of 1.70%) as shown in

----

Figure 8(a). The failure process and failure mode at the confining stress of 12.5kPa have similar results, the V-type shear zone is formed from the edge to the internal zone of the sample, and the only difference is that the V-type shear zone moves a short distance to the right edge of the sample, as shown in Figure 8(b). When the confining stress is 25.0kPa, the V-type shear zone is still observed but move further to the right edge of the sample (see Figure 8(c)). With the further increase of the confining pressure, the V-type shear zone gradually changes to a single shear band at the confining stress of 50kPa, and the single shear band with about 52° along the horizontal direction (see Figure 8(d)). It reveals that V-type shear zone is the main failure mode at the low confining stress. Then the V-type shear zone gradually changes to a single shear band (along the horizontal direction about 52°) with increasing the confining stress. The single shear band with about 52° along the horizontal direction is the main failure mode at the conventional confining stress. Figure 9 compares the simulated failure modes of QH-E lunar soil simulant at different confining stress with the experimental observations. As seen in Figure 9, the failure modes of QH-E by using numerical simulations are in agreement with the experimental observations. These evolution mechanisms of shear band also successfully explain the reason why QH-E lunar soil simulant exhibits a significant strain-softening behaviour in the deviatoric stress versus axial strain curves.
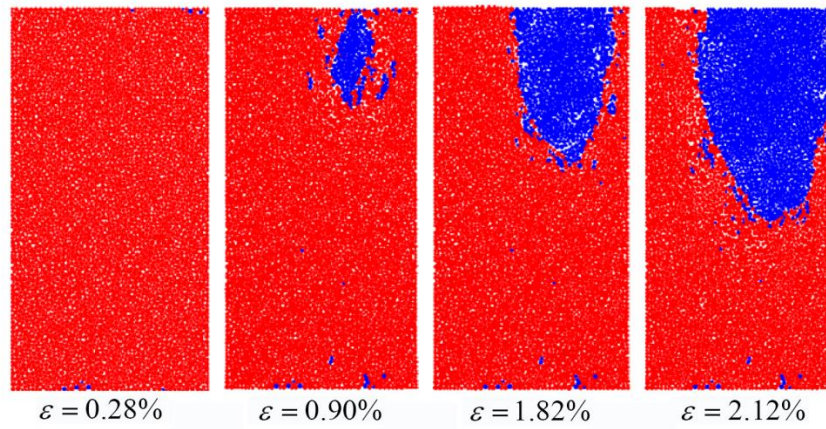

$\varepsilon = 0.2\%$	$\varepsilon = 0.8\%$	$\varepsilon = 1.45\%$	$\varepsilon = 1.70\%$
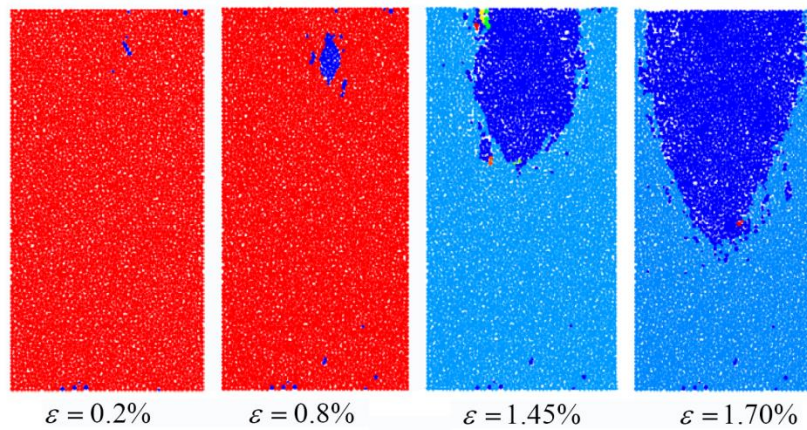
(a) Failure process at the confining stress of 6.25kPa.

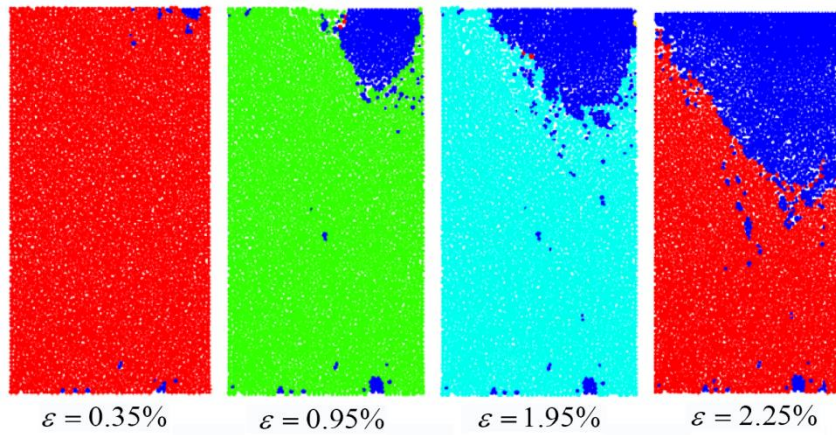|			
$\varepsilon = 0.25\%$	$\varepsilon = 0.85\%$	$\varepsilon = 1.78\%$	$\varepsilon = 2.05\%$

(b) Failure process at the confining stress of 12.5kPa.

Fig. 8 - Failure processes and mechanisms of QH-E lunar soil simulant at different low confining stresses of (a) 6.25kPa, (b) 12.5kPa

$\varepsilon = 0.28\%$ $\varepsilon = 0.90\%$ $\varepsilon = 1.82\%$ $\varepsilon = 2.12\%$

(c) Failure process at the confining stress of 25.0kPa.

$\varepsilon = 0.35\%$ $\varepsilon = 0.95\%$ $\varepsilon = 1.95\%$ $\varepsilon = 2.25\%$

(d) Failure process at the confining stress of 50.0kPa.

Fig. 8 - Failure processes and mechanisms of QH-E lunar soil simulant at different low confining stresses of (c) 25.0kPa, and (d) 50.0kPa .

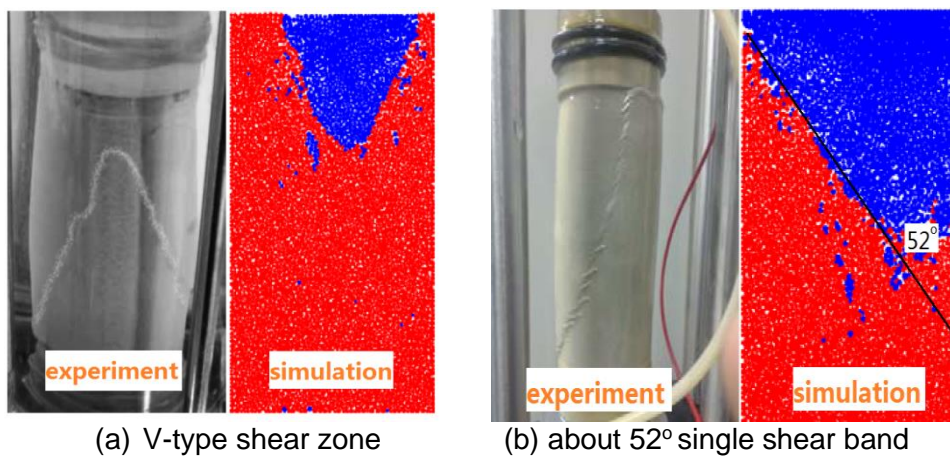(a) V-type shear zone   (b) about 52° single shear band

Fig. 9 - Comparison of Failure modes of QH-E lunar soil simulant between the experimental observation and numerical simulation: (a) V-type shear zone, and (b) about 52° single shear band

----

CONCLUSION

DEM numerical simulations are carried out to investigate the strength properties and failure modes of QH-E lunar soil simulant at the low confining stress. The effects of porosity and friction coefficient on strength properties of QH-E samples are also discussed. The major findings are as follows:

● At low confining stress, the values of peak deviatoric stress, residual stress and axial strain corresponding to the peak stress show an overall good agreement with experimental results, and these values are closer to the experimental values at the lower confining stress. In addition, the deviator stress vs. axial strain and volumetric stress vs. axial strain curves from the present numerical simulations are also similar to those curves from the experimental tests. Therefore, at low confining stress, the proposed model and calibrated microscopic parameters are suitable for simulation the mechanical properties of QH-E lunar soil simulant.

● Both the porosity and friction coefficient can affect the peak strength of QH-E lunar soil simulant, and porosity has a stronger effect on the peak strength for tri-axial compression simulation at low confining stress. The peak stress, residual stress and axial strain corresponding to the peak stress obviously decrease with the increase of the porosity, while these values slightly increase with the increase of the friction coefficient at low confining stress.

● At the low confining stress, the V-type shear zone (double shear bands) is the main failure mode. Then the V-type shear zone gradually changes to a single shear band (along the horizontal direction about 52°) with the increase of the confining stress. These evolution mechanisms of shear band are in agreement with experimental observation and explain the reason that QH-E lunar soil simulant exhibits a significant strain-softening behaviour.

The above results based on DEM simulation provide the important information about the strength properties and failure modes of QH-E lunar soil simulant at the low confining stress. However, it is emphasized that the current results are obtained under a special contact constitutive model without considering the shape and size distribution of actual particles. Due to the QH-E lunar soil simulant of angular shape with sharp corners and a highly irregular surface, a more detailed PFC simulation based on a more suitable constitutive model is necessary for a more accurate understanding of mechanical properties of QH-E lunar soil simulant.

ACKNOWLEDGEMENTS

REFERENCES

[1]   Hasan, A. and Alshibli, K.A. (2010), "Discrete element modeling of strength properties of Johnson Space Center (JSC-1 A) lunar regolith simulant", *Journal of Aerospace Engineering*, **23**(3), 157-165.

[2]   Heiken, G. H., Vaniman,D. T., French, B. M. (1991), "Lunar sourcebook –A user's guide to the moon", Cambridge University Press, Cambridge, U.K., 475-594.

[3]   Carrier, W. D. (2003)."Particle size distribution of lunar soil", *Journal of Geotechnicaland Geoenvironmental Engineering*, **129**(10), 956-959.

[4]   Rickman, D., Hoelzer, H., Carpenter, P., Sibille, L., Howard, R. and Owens, C. (2007), "A quantitative method for evaluating regolith simulants."SpaceTechnology and Applications International Forum-STAIF, *American Institute of Physics*, 957-963.

[5]   Enrique, R., Allen, W., Alan, E., and Carolyn, Y. (2009), "Flow ability of JSC-1A", Research Rep. NASA/TM-2009-215625.

----

[6]   Arslan, H., Batiste, S. and Sture, S. (2010), "Engineering properties of lunar soilsimulant JSC-1A", *Journal of Aerospace Engineering*, **23**(1), 70-83.

[7]   Jiang, M.J., Zheng, M. and Wang, C. (2012), "Distinct element analysis of shear band of lunar soil in biaxial tests", *Rock and Soil Mechanics*, **33**(12), 3801-3809. (in Chinese)

[8]   Jiang, M.J. and Shen, Z.F. (2013), "Thornton C. Microscopic contact model of lunar regolith for high efficiency discrete element analyses", *Computers and Geotechnics*, **54**, 104-116.

[9]   Somrit, C. and Nakagawa, M. (2006), "Simulation of agglutinates formation", *Earth and Space*, **188**(35), 1-7.

[10]   Tryana, V.G. and Masami, N. (2008), "Modeling of agglutinates and its mechanical properties", *Earth and Space 2008: Engineering, Science, Construction, and Operations in Challenging Environments. Long Beach: ASCE*, 1-8.

[11]   Lee, S.J., Hashashi, Y.M.A., Wilkinson, R.A. and Agui, J.H. (2010), "Simulation of experimental tests on the JSC-1A lunar soil simulant with polyhedral discrete elements", *Earth and Space*, 208-216.

[12]   Katagirl, J., Matsushima, T., Yamada, Y., Tsuchiyama, A., Nakano, T., Uesugi, K., Ohtake, M. and Saiki, K. (2015), "Investigation of 3D grain shape characteristics of lunar soil retrieved in Apollo 16 using image-based discrete-element modeling", *Journal of Aerospace Engineering*, **28**(4), 04014092.

[13]   Matsushima, T., Katagiri, J., Uesugi, K., Tsuchiyama, A. and Nakano, T. (2006), "Image-based modeling of lunar soil simulant for 3D DEM simulations", *Earth and Space 2006: Engingeering, Construction, and Operations in Challenging Environment. Houston: ASCE*, 1-8.

 [14]   Matsushima, T., Katagiri, J., Uesugi, K., Tsuchiyama, A. and Nakano, T. (2009), "3D shape characterization and image-based DEM simulation of the lunar soil simulant FJS-1", *Journal of Aerospace Engineering*, **22**(1), 15-23.

[15]   Nakashima, H., Fujii, H., Oida, A., Momozu, M., Kanamori, H., Aoki, S., Yokoyama, T., Shimizu, H., Miyasaka, J. and Ohdio, K. (2010), "Discrete element method analysis of single wheel performance for a small lunar rover on sloped terrain", *Journal of Terramechanics*, **47**, 307-321.

[16]   Knuth, M.A., Johnson, J.B., Hopkins, M.A., Sullivan, R.J. and Moore, J.M. (2012), "Discrete element modeling of Mars Exploration Rover wheel in granular material", *Journal of Terramechanics*, **49**, 27-36.

[17]   Smith, W. and Peng, H. (2013), "Modeling of wheel-soil interaction over rough terrain using the discrete element method", *Journal of Terramechanics*, **50**, 277-287.

[18]   Zou, M., Fan, S.C., Shi, R.Y., Yang, Y.J. and Li, J.Q. (2015), "Effect of gravity on the mechanical properties of lunar regolith tested using a low gravity simulation device", *Journal of Terramechanics*, **60**, 11-22.

[19]   Li, W., Huang, Y., Cui, Y., Dong, S.J. and Wang, J. (2010), "Trafficability analysis of lunar mare terrain by means of the discrete element method for wheeled rover locomotion", *Journal of Terra-mechanics*, **47**(3), 161-172.

[20]   Alshibli, K. A. and Hasan, A. (2009), "Strength Properties of JSC-1A Lunar Regolith Simulant", *Journal of Geotechnical and Geoenvironmental Engineering*, **135**, 673-679.

[21]   Klosky, J.L., Sture, S., Ko, H.Y. and Barnes, F. (2000), "Geotechnical Behavior of JSC-1 Lunar Soil Simulant", *Journal of Aerospace Engineering*, **13**(4), 133-138.

[22]   Nakashima, H., Shioji, Y., Tateyama, K., Aoki, S., Kanamori, H. and Yokoyama, T. (2008), "Specific cutting resistance of lunar regolith simulant under low gravity conditions", *Journal of Space Engineering*, **1**(1), 58-68.

[23]   Yu, H. and Hu, Z. (2014), "Mechanical characteristics of a lunar regolith simulant at low confining pressure", *Environmental Earth Sciences*, **71**, 3697–3703.

[24]   Zou, W. L., Li, Y.L., Cheng, L., Zhang, J.F. and Wang, X.Q. (2016), "Mechanical properties of QH-E lunar soil simulant at low confining stresses", ASCE, Journal of Aerospace Engineering, **29**(2), 04015036.

[25]   Belheine, N., Plassiard, J.P., Donzé, F.V., Darve, F. and Seridi, A. (2009), "Numerical simulation of drained triaxial test using 3D discrete element modeling", *Computers and Geotechnics*, **36**(1-2), 320-331.

[26]   Willman, B.M., Boles, W.B., McKay, D.S. and Allen, C.C. (1995), "Properties of Lunar Soil Simulant JSC-1", *Journal of Aerospace Engineering*, **8**(2), 77–87.

[27]   Hicher, P.Y. and Chang, C.S. (2008), "A constitutive model for lunar soil", *Earth and Space*, 3-8.

----

[28]   Jiang, M.J., Yu, H.S. and Harris, D. (2005), "A novel discrete model granular material incorporating rolling resistance", *Computers and Geotechnics*, **32**(4), 340-357.

[29]   Zou, M., Li, J.Q., Jia, Y., Ren, L.Q. and Li, Y.W. (2008), "Statics characteristics of lunar soil by DEM simulation", *Journal of Jilin University*, **38**(2), 383-387. (in Chinese)

 [30]   Zhao, T., Dai, F., Xu, N.W, Liu, Y. and Xu, Y. (2015), "A composite particle model for non-spherical particles in DEM simulations", *Grannular Matter*, **17**, 763-774.